

# Dynamics of Strong Coupling between CdSe Quantum Dots and Surface Plasmon Polaritons in Subwavelength Hole Array

Hai Wang,<sup>†</sup> Hai-Yu Wang,<sup>\*,†</sup> Andrea Toma,<sup>‡</sup> Taka-aki Yano,<sup>§</sup> Qi-Dai Chen,<sup>†</sup> Huai-Liang Xu,<sup>†</sup> Hong-Bo Sun,<sup>\*,†</sup> and Remo Proietti Zaccaria<sup>\*,‡,||</sup>

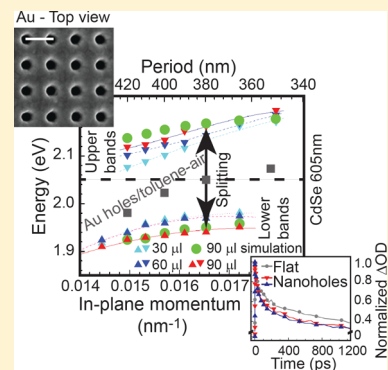
<sup>†</sup>State Key Laboratory on Integrated Optoelectronics, College of Electronic Science and Engineering, Jilin University, Changchun 130012, China

<sup>‡</sup>Istituto Italiano di Tecnologia, via Morego 30, 16163 Genova, Italy

<sup>§</sup>School of Materials and Chemical Technology, Tokyo Institute of Technology, Yokohama, Kanagawa 226-8502, Japan

<sup>||</sup>Cixi Institute of Biomedical Engineering, Ningbo Institute of Materials Technology and Engineering, Chinese Academy of Sciences, Ningbo 315201, China

**ABSTRACT:** We have investigated the strong coupling interaction between excitons of CdSe quantum dots (QDs) and surface plasmon polaritons (SPPs) of gold nanohole array by steady-state spectroscopic method and transient absorption measurements. Numerical and experimental steady-state measurements demonstrate that the SPP–QD system can indeed undergo strong coupling, characterized by a Rabi splitting up to 220 meV. In particular, it is found that in the transient absorption spectra, under resonant excitation, the 1S transition bleaching band from uncoupled CdSe QDs is completely separated into two distinctive bleaching bands, remarkably fingerprinting the hybrid SPP–QD state. It was also found that the lifetime of these hybrid bands is just slightly shorter than the lifetime of bare CdSe QDs, possibly caused by the phonon bottleneck effect due to the large Rabi splitting. These results could open a new avenue toward the development of novel nanoplasmon devices with strong SPP–QD interaction.



The interaction of quantum emitters with surface plasmon polaritons (SPPs) has attracted tremendous attention due to the possibility of controlling light–matter interactions on the nanoscale.<sup>1,2</sup> To date, the exciton–SPP interaction has been especially used to enhance the fluorescence of emitters and to affect the reciprocal energy-transfer rates.<sup>3,4</sup> However, most of the applications take place in the weak-coupling regime, where the interaction only modifies the radiative decay rate of the excitons, while the wave functions of the emitters and SPP modes are considered to be only slightly altered. Conversely, when the interaction is strong enough, striking change of emission properties occurs. Under this condition, the system enters a strong coupling regime where the wave functions of the initial excitonic and surface plasmon states are coherent superpositions. The excitation energy is then coherently exchanged between the emitter and the SPP modes, resulting in the formation of new hybrid bands separated by an energy equal to the Rabi-splitting  $\hbar\Omega_R$ , a quantity proportional to the strength of the light–matter interaction.<sup>5–7</sup>

On the basis of the rotating-wave approximation (RWA),<sup>8</sup> theory predicts that for an individual two-level emitter at resonance with electromagnetic field  $\vec{E}$  and in absence of dissipation, the Rabi splitting is given by<sup>9</sup>

$$\hbar\Omega_R = 2\vec{E}\cdot\vec{d}\sqrt{n_{\text{ph}} + 1} = 2\sqrt{\frac{\hbar\omega}{2\epsilon_0 V}}d\sqrt{n_{\text{ph}} + 1}$$

where  $\hbar\omega$  is the SPPs resonance energy,  $\vec{d}$  is the molecular transition dipole moment of the two-level oscillator,  $\epsilon_0$  is the vacuum permittivity,  $V$  is the modal volume, and  $n_{\text{ph}}$  refers to the number of photons in the system. Furthermore, for a many emitters ( $N$ ) system, the Rabi splitting is proportional to the square root of the molecular concentration  $\sqrt{N/V}$ ,<sup>7,10</sup> where  $N$  is the number of coupled molecules in the SPP modal volume  $V$ .

A strong SPP–exciton coupling regime has been achieved with various kinds of optically active materials such as J-aggregates,<sup>7,11–16</sup> organic dye molecules,<sup>10,17,18</sup> and laser dyes.<sup>19</sup> However, organic molecules tend to photobleach under high optical intensities.<sup>20,21</sup> When this effect turns into an issue, the choice of materials free from this kind of problematic is then mandatory. In this regard, semiconductor nanocrystals, also referred to as quantum dots (QDs), are surely a viable solution.

QDs are a versatile class of materials that exhibit interesting size-dependent optical properties. They display excellent photostable and high photoluminescence quantum yields,<sup>20,21</sup> making them intriguing candidates for various fields of application, especially for nanoplasmonic devices.<sup>22,23</sup> Recently, progress has been made in strong coupling with QDs.<sup>24–26</sup> For

Received: September 8, 2016

Accepted: November 2, 2016

Published: November 2, 2016

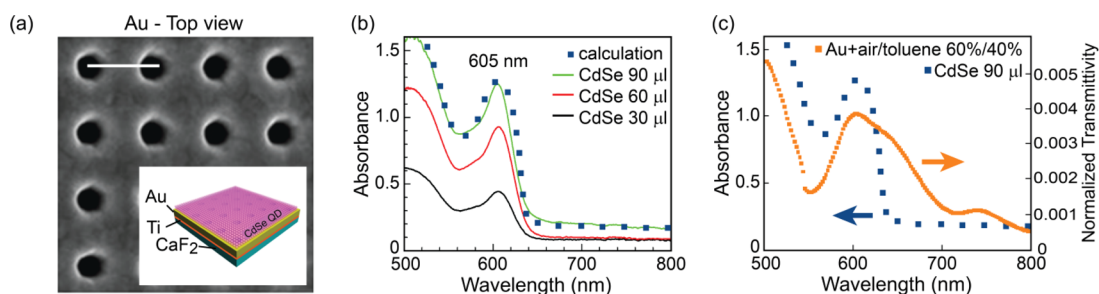


**Figure 1.** (a) Scanning electron microscope image of top-down fabricated hole-based hybrid nanostructure. The white bar indicates the period of the lattice. The inset shows the overall device: a layer of CdSe QDs on top of 200 nm thick layer of squared patterned gold, followed by 5 nm of Ti and a thick layer of CaF<sub>2</sub>. (b) Steady-state experimental absorbance spectra of CdSe QDs film drop-casted on a glass substrate. Three different amounts of CdSe QDs/toluene solutions are considered: 30, 60, and 90 μL (continuous lines). Calculation were also performed to reproduce the CdSe QD absorbance for the 90 μL solution (dot curve). (c) Absorbance spectrum for 90 μL solution overlapped to the transmission spectrum (continuous orange line) obtained by the hybrid structure without the use of CdSe QDs. The structure is formed by a layer of toluene mixed with air, on top of a gold square-like patterned film with period 380 nm, followed by Ti and CaF<sub>2</sub>. Both spectra show maxima at ~605 nm to realize the strong coupling condition.

instance, strong coupling between CdSe QDs and a SPPs on a planar silver thin film has been carried out and characterized by a Rabi splitting of 112 meV.<sup>26</sup> The same authors then reported about transient experiments on QD–SPP hybrid system, which was performed under nonresonant excitation conditions by the Kretschmann geometry reflectometry.<sup>25</sup> However, so far little is known about the kinetics of hybrid systems generated by the interaction of QDs and SPPs. In particular, the dynamics of QD–SPP systems under resonant excitation have not been reported yet, the achievement which would improve the current knowledge on their photophysical essence. In the present work, we demonstrate that strong exciton–SPP coupling can be achieved with CdSe QDs and SPPs supported by gold nanohole array. Furthermore, by ultrafast pump–probe approach, the formation in the transient absorption (TA) spectra of the hybrid bands is clearly shown. Under resonant excitation, we demonstrate that the lifetime of the hybrid state is just slightly shorter than the lifetime of bare QDs.

**Sample Fabrication and Steady-State Measurements.** We chose a golden layer patterned with a sequence of holes following a square-like configuration as SPP device. The process started with the evaporation of 200 nm of gold on a calcium fluoride (CaF<sub>2</sub>) substrate. Afterward, holes covering an overall area of 200 × 200 μm<sup>2</sup> were milled by following a square pattern in the gold films using a focused ion beam apparatus (FEI/Helios Nanolab 650). The ratio between the lattice period and the hole diameter was kept constant at 2.5 with the period falling in the range between 350 and 420 nm. Typically, these kinds of subwavelength metallic hole array structures possess an extraordinary transmission in the optical regime, which nicely demonstrates that the incident light can indeed be turned into SPPs.<sup>27,28</sup>

After the fabrication of the gold layer, a few hundreds of nanometers of CdSe QDs were drop-casted onto the patterned substrates as illustrated in the inset of Figure 1a. The CdSe QDs, as the most extensively investigated colloidal II–VI semiconductor nanoparticles, were purchased in toluene solution from NN-laboratories. With interesting properties such as band gap throughout the visible range and relatively easy synthesis, CdSe QDs have been used in a wide range of applications such as light-emitting devices,<sup>29,30</sup> solar cells,<sup>31,32</sup> photocatalysis, and biological labeling.<sup>33,34</sup> In particular, with a constant concentration of CdSe QDs in toluene equal to 5 mg/mL, we considered three situations corresponding to three

different amounts of CdSe QDs/toluene solution: 30, 60, and 90 μL. The associated absorbance profiles are shown in Figure 1b.

The SPP resonant wavelength is mainly determined by the structure period, which provides the necessary momentum and energy-matching conditions. For a square hole array of period  $P$  at normal incidence, the transmittance spectra peak  $\lambda_{\max}$  is given by the following equation<sup>35–37</sup>

$$\lambda_{\max} \sqrt{i^2 + j^2} = P \sqrt{\frac{\epsilon_m \epsilon_d}{\epsilon_m + \epsilon_d}}$$

where  $\epsilon_m$  and  $\epsilon_d$  are the permittivity of the metal and dielectric media, respectively. Each set of indices ( $i, j$ ) is associated with a peak in the transmission spectrum. Notice that the peak position is influenced by the refractive index of the dielectric media in contact with the metal surface. Thus for CdSe QDs drop-casted structures it is extremely challenging to retrieve the exact SPPs resonance peak from static spectra measurements owing to the CdSe QDs absorption or the influence of toluene at the same spectrum region. Recalling that the main ingredient necessary for the occurrence of strong coupling is the spectral overlapping between the maximum SPPs transmission and the CdSe QD absorbance peak, we have to notice that in the considered period range the combination of just air, as top layer, with a square-like patterned golden structure would provide an SPP peak strongly blue-shifted with respect to the 605 nm absorbance peak of CdSe QDs. In turn, it would mean no strong coupling. In this regard, we have then numerically determined the role of both CdSe QDs, in terms of the real part of the refractive index  $n_{\text{real, CdSe}}$  and toluene (which, we recall, form the solution drop-casted on top of the patterned gold hole array structure) in bringing the SPP peak toward the 605 nm position. By reconstructing the optical properties of CdSe QDs from their absorbance profile shown in Figure 1b (this was done for the 90 μL configuration, but the same applies to the other two cases), we could determine that  $n_{\text{real, CdSe}}$  alone does not allow for a proper overlapping between the SPPs and the 605 nm peak. (This conclusion was reached by considering a uniform layer of CdSe on top of gold.) Thus the next step was to verify the role of toluene. In this process we had, however, to take into account its evaporation characteristic; therefore, the idea of having a uniform layer of toluene on top of gold had to evolve by considering a mixture of air and toluene. Upon TA measurements (see the next section) we could determine an

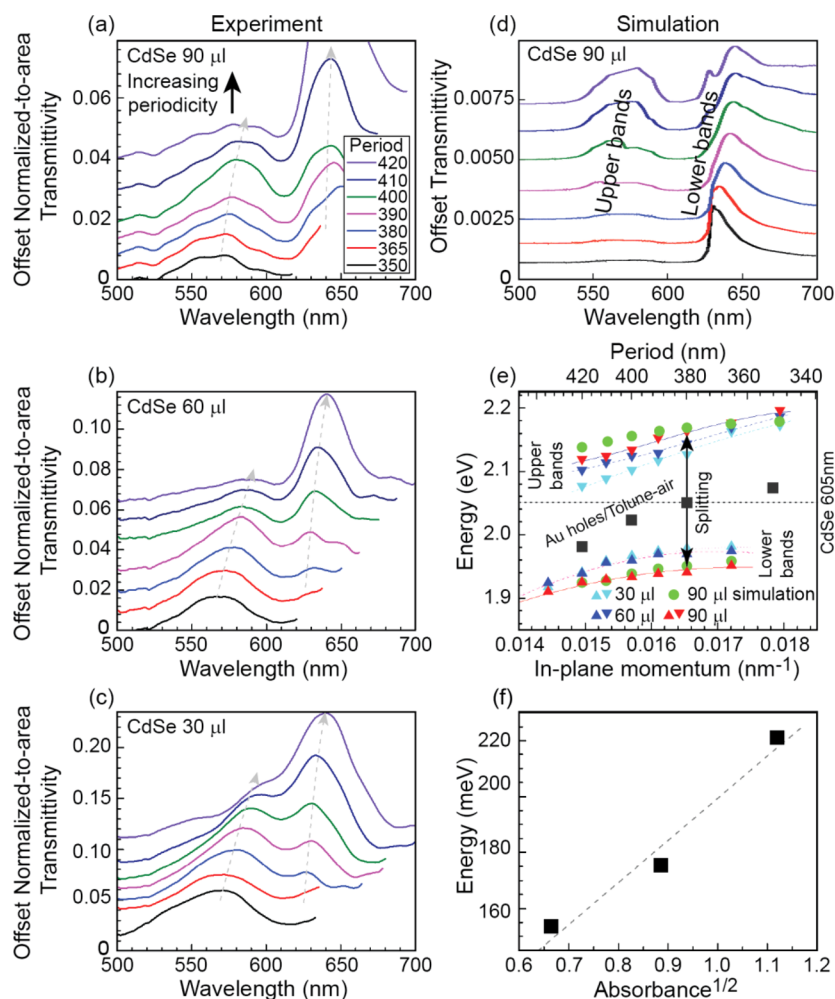


**Figure 2.** Normalized-to-area transmission experimental spectra of a set of hybrid structures drop-casted with CdSe QDs solutions of different amounts: (a) 90, (b) 60, and (c) 30  $\mu\text{L}$ . The periods of the gold hole array vary from 350 to 420 nm. (d) Simulated lower and upper bands for the hybrid structure when the 90  $\mu\text{L}$  solution is considered. The same periodicities as in panel a were considered. (e) Experimental energy dispersion curves showing the lower and upper bands by varying the CdSe QDs solution amounts. The Rabi splitting is estimated around 380 nm period (highlighted by the arrow). The horizontal dotted line describes the CdSe QD absorbance maximum, namely, the 1S exciton transition (see Figure 1b). The gray/square symbols represent the plasmonic behavior obtained through calculations. A similar approach was used to determine the splitting for the 90  $\mu\text{L}$  solution (green circles). (f) Experimental Rabi splitting values as a function of the square root of the CdSe QD film absorbance.

ideal strong coupling period around 380 nm. Hence, to realize a proper overlapping between the SPPs transmission maximum and the 1S transition of the CdSe QDs<sup>38</sup> at 605 nm, we modified the respective concentration of air/toluene reaching an optimum value of 60/40% (which provides an effective refractive index equal to 1.20). Similarly, with respect to the gold optical constants, its description was taken from Alabastri et al.<sup>39</sup> The results are shown in Figure 1c.

Experimental absorbance spectra of the drop-casted CdSe films on bare glass are shown in Figure 1b. As determined by the first exciton transition 1S [1S(e)–1S<sub>3/2</sub>(h)] at 605 nm, where 1S(e) and 1S<sub>3/2</sub>(h) represent the lowest electron (e) and hole (h) levels, the estimated diameter of the CdSe NCs is  $\sim 5$  nm.<sup>38</sup> With increasing of the CdSe/toluene solution amount (30, 60, 90  $\mu\text{L}$ ), the CdSe film absorbance values at 605 nm are found to be 0.45, 0.93 and 1.25, respectively. The normal incidence experimental transmission spectra, acquired when the three different amounts of CdSe solutions are deposited on the gold nanohole array substrate, are plotted in Figure 2a–c.

As it can be seen, two new SPP–QD hybrid bands are formed, both of which continuously red-shift as the lattice period increases from 350 to 435 nm. The dispersion of the separation between the peaks is plotted as a function of the lattice period in Figure 2e. The plot shows a clearly strong coupling characteristic: anticrossing of the hybrid bands,<sup>7</sup> whose magnitude increases with the increasing concentration of CdSe QDs. Under the resonance condition with lattice period of 380 nm, a Rabi splitting up to 220 meV is achieved in the sample with the highest CdSe QD concentration (90  $\mu\text{L}$ ). In support of the aforementioned experimental data, calculations were also performed for the 90  $\mu\text{L}$  solution configuration. The considered numerical approach is based on the RCWA method, which is very suitable for determining the transmission spectrum of 3D structures with 2D periodicity.<sup>14</sup> Furthermore, convergence analysis was performed to guarantee a simulation error below 1%. In particular, Figure 2d shows the calculated transmission peaks forming the upper and lower bands upon period change, while the green circles in Figure 2e remarkably agree with the corresponding experimental data (green circles:

simulations; red triangle: experiment). The same Figure also shows both the 605 nm CdSe QD absorbance resonance (horizontal dotted line) and the SPP behavior when a 60/40% air/toluene mixture is considered on top of the patterned gold layer (square black dots). The crossing of these two lines falls at the periodicity of 380 nm, corresponding to the Rabi splitting position upon drop-casting of CdSe QDs on top of the patterned gold. Finally, the plot of the Rabi splitting values as a function of the square root of the CdSe QDs absorbance is shown in Figure 2f. Importantly, the observed linear relationship shows very good agreement with the expectation for strong coupling regime.<sup>7,40</sup>

Above all, steady-state measurements indicate that the SPP–QD system can undergo strong coupling. To gain further insight into the formation of the hybrid state, TA spectroscopy was also performed.

**Transient Absorption Experiments.** The considered ultrafast femtosecond TA setup<sup>41,42</sup> is based on a mode-locked amplified Ti:sapphire laser system (RGA, Spitfire, Spectra Physics). The output of the laser provides a 250 Hz repetition rate with pulse energy of 1.5 mJ, 100 fs pulse width. Furthermore, at 800 nm wavelength it is divided into two portions to create the pump and probe beams. In particular, the stronger fraction of the pulse is either frequency-doubled by a  $\beta$ -barium borate (BBO) crystal to generate the pump pulses at 400 nm or sent to the TOPAS system to generate desired excitation pulse at 560 nm. The other fraction is instead focused into a sapphire plate to produce a broadband white-light continuum spanning the 450–800 nm wavelength range, used as the probe pulse. Pump and probe pulses are orthogonally collinearly recombined by a dichroic mirror and, through a microscope objective (NA 0.75, magnification 10), focused on the sample at normal incidence. Finally, the relative timing between pump and probe pulses is controlled by a mechanical delay line. Of particular note is that due to the chromatic aberrations, pump and probe beams have different focal planes. Here we optimize the focusing of the probe beam and provide a probed area that is smaller than the nanohole lattice size. Both pulses, which are collected by the same microscope objective, upon interaction with the sample are reflected to a beam splitter, which deviates them toward a spectrometer. In particular, while the pump-associated light is then blocked by a filter, the probe light beam is focused on a fiber-coupled sensitive photodetector (Avantes AvaSpec-2048×14). Another important aspect to consider is the cutoff wavelength due the dichroic mirror used in the present experiment. Indeed, the detection window of the probe light was from 450 to 800 nm under 400 nm laser pulse pump and from 575 to 800 nm under 560 nm pulse pump. Finally, the group velocity dispersion of the transient spectra was compensated by a chirp program.

The 30  $\mu$ L drop-casted CdSe QDs solution (with absorbance values of 0.45 at 605 nm) was chosen for TA measurements. Initially we performed TA experiments under nonresonant conditions by the 400 nm laser pulse, by which electrons were able to pump into thermally excited conduction bands at various energies above the QD conduction band edge. As reference we chose the recorded time-resolved spectra of CdSe QDs drop-casted on a flat gold film, as shown in Figure 3a, which show the typical features of these systems.<sup>43,44</sup> The spectra comprise two bleaching bands peaking at 500 and 590 nm, which can be assigned to the 1P [1P(e)  $\rightarrow$  1P<sub>3/2</sub>(h)] and 1S [1S(e)  $\rightarrow$  1S<sub>3/2</sub>(h)] transitions, respectively. Furthermore, a positive peak was observed at 535 nm resulting from the

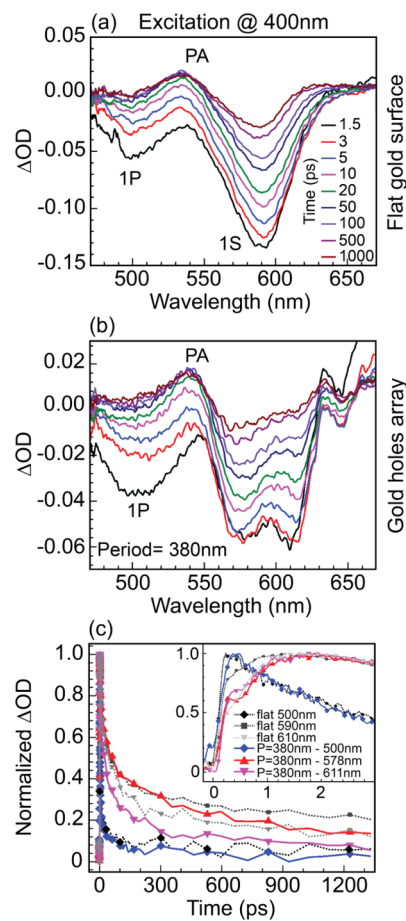


**Figure 3.** Transient absorption spectra under nonresonant 400 nm excitation of CdSe QDs on (a) flat gold film and (b) gold hole array with period equal to 380 nm. The spectra are recorded at 1.5, 3, 5, 10, 20, 50, 100, 500, and 1000 ps. (c) Normalized bleaching dynamics under 400 nm nonresonant excitation of CdSe QDs on flat gold film measured at 500 nm (1P transition, black dotted line), 590 nm (1S transition, gray dotted line), and 610 nm (light-gray dotted line). Similarly, CdSe QDs on gold hole array ( $P = 380$  nm) show a bleaching peak at 500 nm (1P transition, continuous blue line) together with two more peaks at 578 and 610 nm, which are separated by the 1S transition (red and purple continuous lines). The inset shows the dynamics for short time windows.  $\Delta$ OD: optical density variation.

photoinduced absorption (PA) due to the CdSe QDs. The following step was to investigate, always with the nonresonant 400 nm laser pulse, the hybrid structure formed by CdSe QDs on gold hole array. The hole period was chosen as 380 nm to achieve the resonant coupling between SPPs mode and the 1S transition of the CdSe QDs. The TA spectra are shown in Figure 3b. As it can be seen, the 1P absorption band around 500 nm is unchanged with respect to Figure 3a. This result was expected because the 1P transition does not couple to the SPPs resonance. Conversely, there is a small dip appearing in the 1S bleaching band. The dip between the two new peaks corresponds to the 1S transition wavelength of the CdSe QDs. However, the separation between these peaks is very small, even smaller than the results obtained from the steady-state experiment, which suggests that the intrinsic photophysics of the hybrid state cannot be properly described under nonresonant excitation. This condition does indeed imply the excitation of electrons to thermally excited conduction bands,

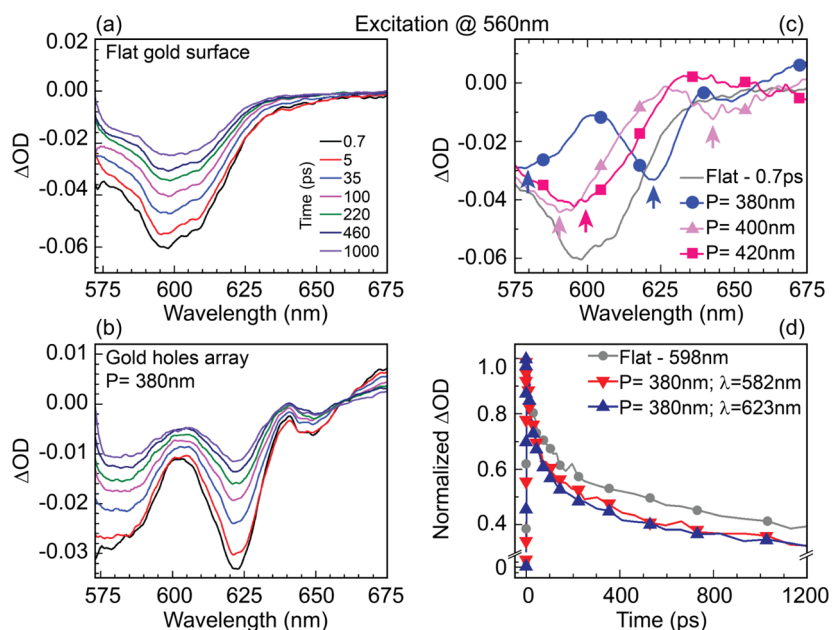


**Figure 4.** TA spectra under 560 nm resonant excitation of CdSe QDs on (a) flat gold film and (b) gold hole array with period 380 nm. The spectra were recorded at 0.7, 5, 35, 100, 220, 460, and 1000 ps. (c) TA spectra measured at 0.7 ps for CdSe QDs drop-casted on a flat gold film and gold hole array with three different periods. The arrows highlight the hybrid peaks. (d) Normalized bleaching dynamics under 560 nm resonant excitation of CdSe QDs on a flat gold film (measured at 598 nm) and on a gold hole array structure of  $P = 380$  nm (measured at the hybrid bands of 582 and 623 nm).

which provide information on the hot electrons relaxation in hybrid systems. Thus the corresponding relaxation dynamics are compared in Figure 3c. (The inset shows dynamics for short time windows.) In particular, the dotted lines describe the kinetic traces at 500, 590, and 610 nm of QDs on flat gold film. The Figure shows that the 1P bleach band at 500 nm grows and also relaxes faster (black square line) than the other bands. As the 1P band starts decreasing ( $\sim 300$  fs), the 1S band at 590 nm shows a slowing down in the initial rise, which has been indicated as relaxation of the 1D and 1P electrons into the lower 1S state. After this state-filling process, the 1S band shows a slow decay (approximately nanoseconds).<sup>45</sup> The kinetics of the hybrid state is also plotted in Figure 3c as solid lines. It is observed that the 1P band dynamic is nearly the same as that of QDs on flat gold film because this transition is not coupled to the SPPs modes. Besides, the dynamics corresponding to the two peaks originating from the 1S bands show a fast initial rise ( $\sim 100$  fs) owing to biexciton effect,<sup>44</sup> followed by a bend, which is caused by a slow increase in the 1S population electron states. The bend reaches the maximum at  $\sim 1.5$  ps to follow with a slow decay. This dynamic process is almost the same as bare QDs at 610 nm. Above all, these similar dynamic processes indicate that electrons located in thermally conduction states can relax into the hybrid bands, suggesting that the state-filling effect is unaffected by the strong coupling. Nonetheless, these results from nonresonant excitation cannot provide information about the intrinsic photophysics of the hybrid state.

To obtain a deeper understanding of the photophysics of the hybrid state, we further performed TA measurements under resonant condition by 560 nm laser pulse, which corresponds to the upper band excitation. Figure 4a shows the TA spectra of CdSe QDs on top of a flat gold film, which was once again chosen as reference. The Figure illustrates one bleaching peak appearing around 600 nm, which is assigned to the 1S

transition of CdSe QDs, similarly to the 400 nm excitation condition. On the contrary, the TA spectra of hybrid structures formed by CdSe QDs drop-casted on gold hole array (period = 380 nm) show totally different features (see Figure 4b). The 1S transition bleaching band is completely separated into two distinctive bleaching signatures with equal intensities, a result that remarkably underlines the formation of the hybrid state. The two peaks located at 580 and 622 nm show a Rabi splitting energy as 145 meV, which is consistent with the value measured from steady-state experiments.

Importantly, we performed TA measurements under resonant condition also on hybrid structures of CdSe QDs drop-casted on gold hole array structures having different periods. In this case, the TA spectra recorded at maximum amplitude are plotted in Figure 4c. As the hole period increases from 380 to 400 nm, both of the two bands show a red shift, resulting in accordance with the static measurements (Figure 2). The intensities of the two bands are no longer equal, indicating that the strength of the coupling becomes weaker. With further increasing of the period to 420 nm (pink line), the splitting peaks are not detectable any longer because the SPP mode and the 1S transition of the CdSe QDs have become off-resonant. Therefore, through varying the period of the hole array in TA measurements, it can be clearly observed that when the nanohole array period is equal to 380 nm, the SPP resonance can overlap with the first exciton transition of the CdSe QDs. Finally, it is worth noticing the absence of any positive signals in the TA spectra, suggesting that the intrinsic nonthermal decay of the hybrid state should be properly represented under resonant excitation.

In terms of dynamics and always assuming resonant excitation condition, we compared the normalized results of the upper and lower hybrid bands under the strongest coupling regime ( $P = 380$  nm) with the behavior from bare excitons of CdSe QDs on a flat gold film. As shown in Figure 4d, the

lifetime of the hybrid bands is slightly shorter than for bare excitons. To analyze this result, we have to recall that in strong coupling regime the hybrid system is a combination of excitons and SPPs components. In general, the lifetime of hybrid states is expected to be governed by fast decay mechanisms, namely, the damping of SPP modes, which is in the range of tens of femtoseconds.<sup>46,47</sup> Here the lifetime of the hybrid bands is instead only slightly slower than that for bare CdSe QDs (approximately nanoseconds); indeed it is much longer than the typical SPPs damping time. Thus the kinetics of the hybrid bands cannot be defined in any simple way.

Specifically, recent experiments have demonstrated that the lifetime of hybrid systems with J-aggregates can be intrinsically long. In particular, it was found that the phonon bottleneck effect can play a key role in such mechanism.<sup>48,49</sup> In the present situation, because of the spatial confinement, well-defined energy levels are induced in the QDs. If the spacing among the energy levels is large enough, the rate of carrier relaxation will be strongly reduced due to the mismatch between the electronic gaps and phonon frequencies. In other words, the bottleneck effect is responsible for suppressing the vibrational relaxation levels, as already demonstrated in the state filling of semiconductor QDs.<sup>50</sup> Therefore, by assuming that the transition from the upper to lower band is mediated by relaxation through multivibrational modes, under the condition of a large Rabi splitting the transition will be inhibited due to the phonon bottleneck effect, allowing for an increase in the upper hybrid band relaxation time. As a result of the phonon bottleneck effect, the lifetime of hybrid states can be very long and only slightly shorter than bare QDs.

We have constructed a hybrid structure by drop-casting CdSe QDs on a gold subwavelength hole array and demonstrated that strong coupling can be achieved with SPP modes and excitons of CdSe QDs. Numerical calculations were also implemented for a better insight into the system. A large Rabi splitting energy up to 220 meV is obtained. Furthermore, the photophysics of the formed hybrid state was studied by ultrafast pump-probe approach. Under nonresonant excitation, we have demonstrated that state-filling effect is unaffected by the strong coupling. Furthermore, under resonant excitation, the formation of the hybrid state is remarkably displayed in the TA spectra, where the nonthermal decay was also directly represented. We have found a slow decay of the hybrid state lifetime, with it being just slightly shorter than the lifetime of bare CdSe QDs. As a possible explanation we have suggested the phonon bottleneck effect due to the large Rabi splitting. To conclude, this work provides a theoretical framework for realizing, through the use of QDs, novel active nanoplasmonic devices such as ultrafast all-optical switches/modulators or nanolasers.

## AUTHOR INFORMATION

### Corresponding Authors

\*H.-Y.W.: E-mail: haiyu\_wang@jlu.edu.cn.

\*H.-B.S.: E-mail: hbsun@jlu.edu.cn.

\*R.P.Z.: E-mail: remo.proietti@iit.it.

### Notes

The authors declare no competing financial interest.

## ACKNOWLEDGMENTS

We acknowledge National Basic Research Program of China (973 Program, Grant No. 2014CB921300), Natural Science

Foundation China (NSFC) under Grant nos. 21273096 and 21473077, and Doctoral Fund Ministry of Education of China under Grant no. 20130061110048 for support. Furthermore, we recognize the support from the Ningbo 3315 Innovative Teams Program, China.

## REFERENCES

- (1) Achermann, M. Exciton-Plasmon Interactions in Metal-Semiconductor Nanostructures. *J. Phys. Chem. Lett.* **2010**, *1*, 2837–2843.
- (2) Taminiau, T. H.; Stefani, F. D.; Segerink, F. B.; van Hulst, N. F. Optical Antennas Direct Single-Molecule Emission. *Nat. Photonics* **2008**, *2*, 234–237.
- (3) Okamoto, K.; Niki, I.; Shvarts, A.; Narukawa, Y.; Mukai, T.; Scherer, A. Surface-Plasmon-Enhanced Light Emitters Based on InGaN Quantum Wells. *Nat. Mater.* **2004**, *3*, 601–605.
- (4) Lakowicz, J. R.; Ray, K.; Chowdhury, M.; Szmacinski, H.; Fu, Y.; Zhang, J.; Nowaczyk, K. Plasmon-Controlled Fluorescence: a New Paradigm in Fluorescence Spectroscopy. *Analyst* **2008**, *133*, 1308–1346.
- (5) Lidzey, D. G.; Bradley, D. D. C.; Skolnick, M. S.; Virgili, T.; Walker, S.; Whittaker, D. M. Strong Exciton-Photon Coupling in an Organic Semiconductor Microcavity. *Nature* **1998**, *395*, 53–55.
- (6) Auffèves, A.; Gerace, D.; Richard, M.; Portolan, S.; Santos, M. F.; Kwek, L. C.; Miniatura, C. *Strong Light-Matter Coupling*; World Scientific: Singapore, 2014.
- (7) Dintinger, J.; Klein, S.; Bustos, F.; Barnes, W. L.; Ebbesen, T. W. Strong Coupling between Surface Plasmon-Polaritons and Organic Molecules in Subwavelength Hole Arrays. *Phys. Rev. B: Condens. Matter Mater. Phys.* **2005**, *71*, 035424.
- (8) Jaynes, E. T.; Cummings, F. W. Comparison of Quantum and Semiclassical Radiation Theories with Application to the Beam Maser. *Proc. IEEE* **1963**, *51*, 89–109.
- (9) Haroche, S.; Kleppner, D. Cavity Quantum Electrodynamics. *Phys. Today* **1989**, *42*, 24–30.
- (10) Hakala, T. K.; Toppari, J. J.; Kuzyk, A.; Pettersson, M.; Tikkanen, H.; Kunttu, H.; Törmä, P. Vacuum Rabi Splitting and Strong-Coupling Dynamics for Surface-Plasmon Polaritons and Rhodamine 6G Molecules. *Phys. Rev. Lett.* **2009**, *103*, 053602.
- (11) Bellessa, J.; Symonds, C.; Vynck, K.; Lemaitre, A.; Brioude, A.; Beaur, L.; Plenet, J. C.; Viste, P.; Felbacq, D.; Cambri, E.; et al. Giant Rabi Splitting between Localized Mixed Plasmon-Exciton States in a Two-Dimensional Array of Nanosize Metallic Disks in an Organic Semiconductor. *Phys. Rev. B: Condens. Matter Mater. Phys.* **2009**, *80*, 033303.
- (12) Hao, Y.-W.; Wang, H.-Y.; Jiang, Y.; Chen, Q.-D.; Ueno, K.; Wang, W.-Q.; Misawa, H.; Sun, H.-B. Hybrid-State Dynamics of Gold Nanorods/Dye J-Aggregates under Strong Coupling. *Angew. Chem.* **2011**, *123*, 7970–7974.
- (13) Wang, H.; Wang, H.-Y.; Bozzola, A.; Toma, A.; Panaro, S.; Raja, W.; Alabastri, A.; Wang, L.; Chen, Q.-D.; Xu, H.-L.; et al. Dynamics of Strong Coupling between J-Aggregates and Surface Plasmon Polaritons in Subwavelength Hole Arrays. *Adv. Funct. Mater.* **2016**, *26*, 6197.
- (14) Wang, H.; Toma, A.; Wang, H.-Y.; Bozzola, A.; Miele, E.; Haddadpour, A.; Veronis, G.; De Angelis, F.; Wang, L.; Chen, Q.-D.; et al. The Role of Rabi Splitting Tuning in the Dynamics of Strongly Coupled J-Aggregates and Surface Plasmon Polaritons in Nanohole Arrays. *Nanoscale* **2016**, *8*, 13445–13453.
- (15) DeLacy, B. G.; Miller, O. D.; Hsu, C. W.; Zander, Z.; Lacey, S.; Yagloski, R.; Fountain, A. W.; Valdes, E.; Anquillare, E.; Soljačić, M.; et al. Coherent Plasmon-Exciton Coupling in Silver Platelet-J-Aggregate Nanocomposites. *Nano Lett.* **2015**, *15*, 2588–2593.
- (16) Melnikau, D.; Esteban, R.; Savateeva, D.; Sánchez-Iglesias, A.; Grzelczak, M.; Schmidt, M. K.; Liz-Marzán, L. M.; Aizpurua, J.; Rakovich, Y. P. Rabi Splitting in Photoluminescence Spectra of Hybrid Systems of Gold Nanorods and J-Aggregates. *J. Phys. Chem. Lett.* **2016**, *7*, 354–362.

- (17) Baieva, S.; Hakala, T.; Toppari, J. Strong Coupling between Surface Plasmon Polaritons and Sulforhodamine 101 dye. *Nanoscale Res. Lett.* **2012**, *7*, 191.
- (18) Gambino, S.; Mazzeo, M.; Genco, A.; Di Stefano, O.; Savasta, S.; Patanè, S.; Ballarini, D.; Mangione, F.; Lerario, G.; Sanvitto, D.; et al. Exploring Light–Matter Interaction Phenomena under Ultrastrong Coupling Regime. *ACS Photonics* **2014**, *1*, 1042–1048.
- (19) Valmorra, F.; Bröll, M.; Schwaiger, S.; Welzel, N.; Heitmann, D.; Mendach, S. Strong Coupling between Surface Plasmon Polariton and Laser Dye Rhodamine 800. *Appl. Phys. Lett.* **2011**, *99*, 051110.
- (20) Lichtman, J. W.; Conchello, J.-A. Fluorescence Microscopy. *Nat. Methods* **2005**, *2*, 910–919.
- (21) Resch-Genger, U.; Grabolle, M.; Cavaliere-Jaricot, S.; Nitschke, R.; Nann, T. Quantum Dots versus Organic Dyes as Fluorescent Labels. *Nat. Methods* **2008**, *5*, 763–775.
- (22) Pacifici, D.; Lezec, H. J.; Atwater, H. A. All-Optical Modulation by Plasmonic Excitation of CdSe Quantum Dots. *Nat. Photonics* **2007**, *1*, 402–406.
- (23) Plum, E.; Fedotov, V. A.; Kuo, P.; Tsai, D. P.; Zheludev, N. I. Towards the Lasing Spaser: Controlling Metamaterial Optical Response with Semiconductor Quantum Dots. *Opt. Express* **2009**, *17*, 8548–8551.
- (24) Santhosh, K.; Bitton, O.; Chuntunov, L.; Haran, G. Vacuum Rabi Splitting in a Plasmonic Cavity at the Single Quantum Emitter Limit. *Nat. Commun.* **2016**, *7*, 11823.
- (25) Gómez, D. E.; Lo, S. S.; Davis, T. J.; Hartland, G. V. Picosecond Kinetics of Strongly Coupled Excitons and Surface Plasmon Polaritons. *J. Phys. Chem. B* **2013**, *117*, 4340–4346.
- (26) Gómez, D. E.; Vernon, K. C.; Mulvaney, P.; Davis, T. J. Surface Plasmon Mediated Strong Exciton–Photon Coupling in Semiconductor Nanocrystals. *Nano Lett.* **2010**, *10*, 274–278.
- (27) Ebbesen, T. W.; Lezec, H. J.; Ghaemi, H. F.; Thio, T.; Wolff, P. A. Extraordinary Optical Transmission through Sub-Wavelength Hole Arrays. *Nature* **1998**, *391*, 667–669.
- (28) Genet, C.; Ebbesen, T. W. Light in Tiny Holes. *Nature* **2007**, *445*, 39–46.
- (29) Coe, S.; Woo, W.-K.; Bawendi, M.; Bulovic, V. Electroluminescence from Single Monolayers of Nanocrystals in Molecular Organic Devices. *Nature* **2002**, *420*, 800–803.
- (30) Colvin, V. L.; Schlamp, M. C.; Alivisatos, A. P. Light-Emitting Diodes Made from Cadmium Selenide Nanocrystals and a Semiconducting Polymer. *Nature* **1994**, *370*, 354–357.
- (31) Huynh, W. U.; Dittmer, J. J.; Alivisatos, A. P. Hybrid Nanorod-Polymer Solar Cells. *Science* **2002**, *295*, 2425–2427.
- (32) Sargent, E. H. Colloidal Quantum Dot Solar Cells. *Nat. Photonics* **2012**, *6*, 133–135.
- (33) Alivisatos, P. The Use of Nanocrystals in Biological Detection. *Nat. Biotechnol.* **2004**, *22*, 47–52.
- (34) Palmisano, G.; Augugliaro, V.; Pagliaro, M.; Palmisano, L. Photocatalysis: a Promising Route for 21st Century Organic Chemistry. *Chem. Commun.* **2007**, 3425–3437.
- (35) Barnes, W. L.; Dereux, A.; Ebbesen, T. W. Surface Plasmon Subwavelength Optics. *Nature* **2003**, *424*, 824–830.
- (36) Nishijima, Y.; Nigorinuma, H.; Rosa, L.; Juodkasis, S. Selective Enhancement of Infrared Absorption with Metal Hole Arrays. *Opt. Mater. Express* **2012**, *2*, 1367–1377.
- (37) Nishijima, Y.; Adachi, Y.; Rosa, L.; Juodkasis, S. Augmented Sensitivity of an IR-Absorption Gas Sensor Employing a Metal Hole Array. *Opt. Mater. Express* **2013**, *3*, 968–976.
- (38) Yu, W. W.; Qu, L.; Guo, W.; Peng, X. Experimental Determination of the Extinction Coefficient of CdTe, CdSe, and CdS Nanocrystals. *Chem. Mater.* **2003**, *15*, 2854–2860.
- (39) Alabastri, A.; Tuccio, S.; Giugni, A.; Toma, A.; Liberale, C.; Das, G.; Angelis, F.; Fabrizio, E.; Zaccaria, R. Molding of Plasmonic Resonances in Metallic Nanostructures: Dependence of the Non-Linear Electric Permittivity on System Size and Temperature. *Materials* **2013**, *6*, 4879–4910.
- (40) Salomon, A.; Wang, S.; Hutchison, J. A.; Genet, C.; Ebbesen, T. W. Strong Light-Molecule Coupling on Plasmonic Arrays of Different Symmetry. *ChemPhysChem* **2013**, *14*, 1882–1886.
- (41) Wang, L.; Li, Q.; Wang, H.-Y.; Huang, J.-C.; Zhang, R.; Chen, Q.-D.; Xu, H.-L.; Han, W.; Shao, Z.-Z.; Sun, H.-B. Ultrafast Optical Spectroscopy of Surface-Modified Silicon Quantum Dots: Unraveling the Underlying Mechanism of the Ultrabright and Color-Tunable Photoluminescence. *Light: Sci. Appl.* **2015**, *4*, e245.
- (42) Wang, H.; Wang, H.-Y.; Gao, B.-R.; Jiang, Y.; Yang, Z.-Y.; Hao, Y.-W.; Chen, Q.-D.; Du, X.-B.; Sun, H.-B. Surface Plasmon Enhanced Absorption Dynamics of Regioregular Poly(3-hexylthiophene). *Appl. Phys. Lett.* **2011**, *98*, 251501.
- (43) Knowles, K. E.; McArthur, E. A.; Weiss, E. A. A Multi-Timescale Map of Radiative and Nonradiative Decay Pathways for Excitons in CdSe Quantum Dots. *ACS Nano* **2011**, *5*, 2026–2035.
- (44) Klimov, V. I. Optical Nonlinearities and Ultrafast Carrier Dynamics in Semiconductor Nanocrystals. *J. Phys. Chem. B* **2000**, *104*, 6112–6123.
- (45) Wang, H.; de Mello Donegá, C.; Meijerink, A.; Glasbeek, M. Ultrafast Exciton Dynamics in CdSe Quantum Dots Studied from Bleaching Recovery and Fluorescence Transients. *J. Phys. Chem. B* **2006**, *110*, 733–737.
- (46) Hartland, G. V. Optical Studies of Dynamics in Noble Metal Nanostructures. *Chem. Rev.* **2011**, *111*, 3858–3887.
- (47) Pelton, M.; Aizpurua, J.; Bryant, G. Metal-Nanoparticle Plasmonics. *Laser Photonics Rev.* **2008**, *2*, 136–159.
- (48) Bockelmann, U.; Bastard, G. Phonon Scattering and Energy Relaxation in Two-, One-, and Zero-Dimensional Electron Gases. *Phys. Rev. B: Condens. Matter Mater. Phys.* **1990**, *42*, 8947–8951.
- (49) Nozik, A. J. Spectroscopy and Hot Electron Relaxation Dynamics in Semiconductor Quantum Wells and Quantum Qots. *Annu. Rev. Phys. Chem.* **2001**, *52*, 193–231.
- (50) Urayama, J.; Norris, T. B.; Singh, J.; Bhattacharya, P. Observation of Phonon Bottleneck in Quantum Dot Electronic Relaxation. *Phys. Rev. Lett.* **2001**, *86*, 4930–4933.